Supporting Information for: Multistep and multiscale electron transfer and localization dynamics at a model electrolyte/metal interface

Sarah B. King,[1, a)] Katharina Broch,[1, b)] Angelika Demling,[1] and Julia Stähler[1, c)]

Department of Physical Chemistry, Fritz Haber Institute of the Max Planck Society, Faradayweg 4-6, 14195 Berlin, Germany

(Dated: 7 September 2018)

[a)]Present address: University of Chicago, Department of Chemistry and James Franck Institute, 929 E 57th Street, Chicago, IL 60637, USA; Electronic mail: sbking@uchicago.edu

[b)]Present address: Universität Tübingen, Institut für Angewandte Physik, Auf der Morgenstelle 10, 72076 Tübingen, Germany

[c)]Electronic mail: staehler@fhi-berlin.mpg.de

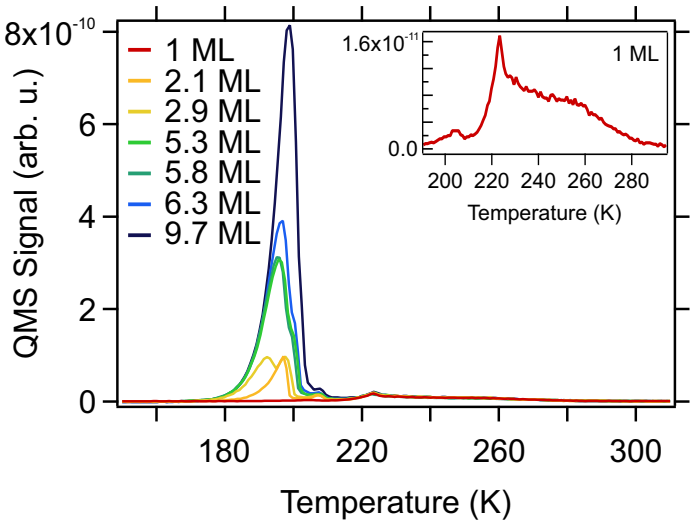

FIG. S1. TPD of 1 to 9.7 ML of DMSO on the Cu(111) surface measuring mass 63 m/z with a desorption rate of 30 K/min. The inset shows the 1 ML region.

I. DMSO DOSING AND TEMPERATURE PROGRAMMED DESORPTION OF DMSO/CU(111)

DMSO was dosed through a pinhole doser with a diameter of 5 μm with a backing pressure of 6 x 10^{-1} mbar. With the Cu crystal at 200 K, DMSO was dosed for 3.5 minutes to ensure an excess of DMSO on the surface and the surface was then annealed to 210 K for 10 minutes. Dosing and annealing of a monolayer was performed at all coverages prior to subsequent dosing. An additional short 30 second dosing at 200 K was necessary for saturation of the first monolayer as verified by temperature programmed desorption (TPD) of DMSO with a heat rate of 30 K/min, shown in Figure S1. The 2 monolayer equivalent coverage (ML equiv.) was deposited by additional dosing at 180 K for 45 seconds. In order to dose coverages higher than 2 ML equiv., DMSO was dosed at 150 K for between 1.5 and 3 minutes depending on desired final coverage and subsequently annealed to 180 K for 10 minutes. This second annealing step is required for distinct spectral features P_1 and P_2. For the 6 ML equiv. coverage the second dosing time at 150 K was 2.25 minutes. There was some variation in coverage with the same dosing time, and therefore all coverages were determined after data acquisition by TPD, shown in Figure S1. The integrated TPD intensity of the major mass fragment from 150 to 400 K at 63 m/z was divided by the integrated TPD for the 1 ML equiv. region between 204 K and 400 K. The theory of TPD is described in detail

in reference S1.

A detailed description of the gas-system and pinhole doser and TPD can be found in German in reference S2. A translation of the relevant passage on page 43 regarding the gas-system is as follows: "The gas system consists of only stainless steel and glass components. The pipe connectors and valves are provided by Swagelok. The valves are bellows-sealed and are, like the entire system, capable of being baked to remove contamination. The system is pumped by it's own turbomulecular pump and can reach a minimum pressure of the low 10^{-7} mbar range." A translation of the relevant passage regarding the pinhole doser on page 43 is as follows: "The dosing device consists of a pinhole doser with a 5 micron diameter attached on the vacuum side via a 22 cm long tube. Just behind the aperture a tantalum pipe is clamped in the tube to block the direct molecular beam. The sample is positioned a few millimeters in front of the tube during dosing. Such a geometric arrangement ensures a homogeneous molecular beam and thus a uniform distribution of the adsorbate on the sample surface. Uniform dosing is confirmed by 2PPE measurements where the adsorbate-induced work function change is independent of the position of the laser beam on the sample."

II. NEGATIVE-TIME BACKGROUND FOR 6 ML

Averaging the time delays between -50 and -7 ps results in the negative-time background spectrum shown by the dotted black line in Figure 2(b) from the main paper. This background spectrum either captures photoemission that is not correlated with pump-probe delay time or photoemission from electronic states with lifetimes longer than the inverse repetition rate of the laser. Three different peaks are observed in the background for the 6 ML film: the static 2PPE of two peaks, P_1 and P_2, pumped and probed by $h\nu_1$, that correspond to intermediate state energies of 2.81 and 2.35 $\pm$ 0.05 eV (right energy axis), respectively, as well as photoemission of P_2, pumped with $h\nu_1$ and probed with $h\nu_2$ (left energy axis). Photoemission from P_2 with $h\nu_2$ occurs at negative pump-probe delay times because P_2 has a lifetime longer than 5 μs. The difference in intensity of P_2 in the static spectra in Figure 1(a) and the negative time background in Figure 2(b) in the main paper is due to a real-time intensity decrease in P_2 with illumination and this effect was mitigated in the time-resolved data collection.[S3]

III. FITTING OF THE TIME-RESOLVED DATA

The XC_1 time-dependent intensities can be fit to equation (S1),

$$XC_1(t) = \mathrm{sech}^2((t-t_0)/\tau) * \begin{cases} A_1 e^{(t-t_0)/\tau_1}, & t \leq t_0 \\ A_2 e^{-(t-t_0)/\tau_2}, & t > t_0 \end{cases} \tag{S1}$$

where the exponential function $t \leq t_0$ captures hot electron dynamics, pumped by $h\nu_2$ and probed by $h\nu_1$, while the exponential $t > t_0$ captures the approximate lifetime of P_1.

At both coverages the integrated intensity of the energy region of P_2 which overlaps with the edge of P_1, XC_2, from Figure 2(c) in the main paper, is fit well with a simple mono-exponential rise and decay: equation (S2). Note this is not referring to the hot electron peak at time-zero, but rather the small peak observed after 100 fs.

$$XC_2(t) = -A_1 e^{-(t-t_0)/\tau_1} + A_2 e^{-(t-t_0)/\tau_2} \tag{S2}$$

For 6 ML the rise-time is 70 ± 60 fs and the decay is 170 ± 90 fs, while for 2 ML the rise-time is 70 ± 40 fs and the decay is 190 ± 70 fs.

The equation for the broken-line fit which captures the two shifting regions of P_1 is:

$$E_{\mathrm{center}}(t) = \begin{cases} s_I(t-t') + E', & t \leq t' \\ s_{II}(t-t') + E', & t > t' \end{cases} \tag{S3}$$

where t' and E' are the time and energy where the peak energy shifting trends change and s_I and s_{II} are the slopes before and after t'.

IV. TIME-RESOLVED 2PPE SPECTRA OF 2 ML OF DMSO ON CU(111)

As in Figure 2 of the main paper for 6 ML, Figure S2(a) shows a time-resolved 2PPE spectrum of 2.1 ML of DMSO on Cu(111) (referred to in the text as 2 ML for ease) as a function of intermediate state energy and pump-probe time delay in false color without background subtraction integrated over $k_{||} = \pm$ 0.06 Å^{-1}. The same 3.08 eV pump pulse and 2.19 eV probe pulse were used and the cross-correlation of the two pulses, fit with a $\mathrm{sech}^2(t/\tau)$ function, is 53 ± 8 fs. The spectra at specific pump-probe time delays as provided in the main paper are shown in Figure S2(b).

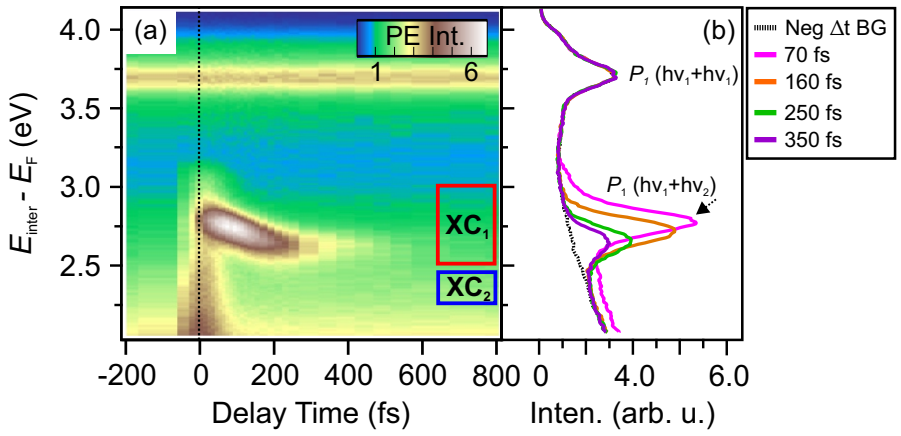

FIG. S2. (a) Time-resolved 2PPE spectrum of 2.1 ML of DMSO on Cu(111) with $h\nu_1 = 3.08$ eV and $h\nu_2 = 2.19$ eV integrated over $k_{||} = \pm\ 0.06$ Å^{-1}. The dotted line shows time-zero and the red and blue rectangles are the integration regions for Figure 4(a) in the main paper. (b) 2PPE spectra at specific pump-probe time delays: the negative time background between -50 to -7 ps, 70 fs, 160 fs, 250 fs, and 350 fs, with the static $P_1(h\nu_1 + h\nu_1)$ and the pump-probe correlated $P_1(h\nu_1 + h\nu_2)$.

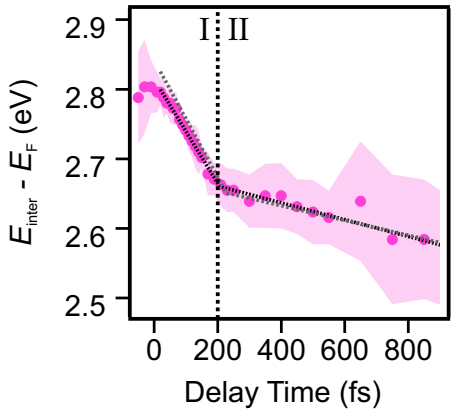

FIG. S3. The peak center of P_1 for 2 ML versus pump-probe time delay and a fit to equation (3) from the main paper. The broken-line fit from the 6 ML data is added for reference in grey.

For 2 ML, the peak energy shifting is within error bars of that for 6 ML, and is shown in Figure S3 including the broken-line fit for the 6 ML data as reference. Fitting this shifting to equation S3, $t' = 210\ \pm\ 30$ fs, $E' = 2.64\ \pm\ 0.02$ eV, $s_I = -0.78\ \pm\ 0.11$ meV/fs and $s_{II} = -0.13\ \pm\ 0.07$ meV/fs. The two regions of shifting are marked by region I and region II.

V. DISPERSION FITTING OF P_1, HIGH $k_{||}$ DATA

Through equation (S4),

$$\hbar k_{||} = \sqrt{2m_e E_{\mathrm{KE}}} \sin\alpha \tag{S4}$$

the angle of photoemission, α, and kinetic energy of the electrons, E_{KE}, can be related to parallel momentum, $k_{||}$, which is conserved upon photoemission. The dispersion of the electronic state is a measure of an electronic states' (de)localization, and is described by equation (S5)

$$E(k_{||}) = E(k_0) + \frac{\hbar^2}{2m^*} k_{||}^2 \tag{S5}$$

using the free-electron approximation where $E(k_0)$ is the energy of the electronic state at $k_{||} = 0$, and m^* is the effective mass of an electron in the electronic state.

Figure S4 shows example Gaussian fits of the center of P_1 as a function of pump-probe delay time and $k_{||}$. A simple Gaussian function,

$$y(x) = A\exp[-4\ln 2(x - x_0)^2/\mathrm{FWHM}^2] + y_0 \tag{S6}$$

with a constant background captures the peak dispersion for all pump-probe delays. At early times, where there is a hot-electron background, y_0 has a non-zero offset while at later delays, where there is no hot-electron background, $y_0 \approx 0$. The dotted pink line in Figure S4 guides the eye to show the positive, flat, and slightly negative dispersion observed at 40, 140, and 200 fs, respectively.

Figure S5 shows angle-resolved data for four different pump-probe time-delay regions, where several delays were averaged together in order to improve the signal-to-noise. These spectra were taken with the sample at $\theta = 10^\circ$ with respect to the hemispherical analyzer, measuring over $\theta = -3^\circ$ to 23° and covering the high angles where Strader *et al.*[S4] see evidence for two separate peaks, one localized and one delocalized. In our data we do not see two clear features, but rather one feature where the dispersion steadily changes. This is particularly clear in Figure S5(c) where there is no hot-electron background congesting the spectra as occurs near time-zero. The red-lines in Figure S5 show dispersion curves, as described by Equation S4, which capture the dispersion of the features well. The effective masses are 1.8, 1.8, 3.4, and -5 for (a)-(d) respectively, taken from the fits of Figure 3(a) in the main paper.

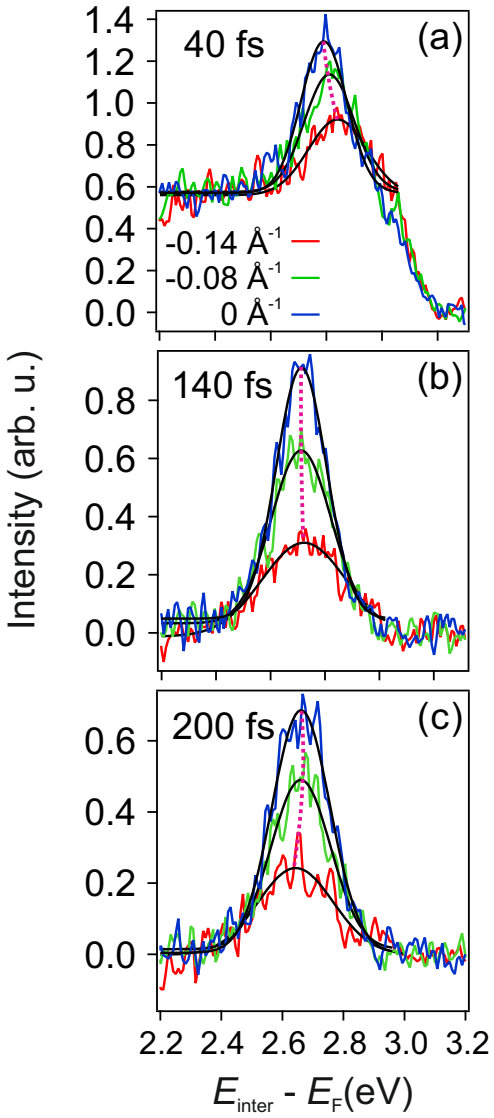

FIG. S4. Gaussian fits of P_1 at representative pump-probe time delays (a) 40 fs, (b) 140 fs, and (c) 200 fs at three different $k_{||}$.

VI. PUMP-WAIT-PROBE MEASUREMENTS OF THE LIFETIME OF P_2

Pump-wait-probe measurements, as described in detail in references,[S5,S6] were used to determine the lifetimes of electronic states that survive longer than the inverse repetition rate of the laser system, 5 μs. Shown schematically in Figure S6, a train of 3.1 eV pulses produce a steady-state population of the long-lived state, after which a mechanical shutter blocks the laser and the long-lived state decays with a rate $1/\tau$. After a known wait time, a second mechanical shutter opens and the remaining electronic population is photoemitted

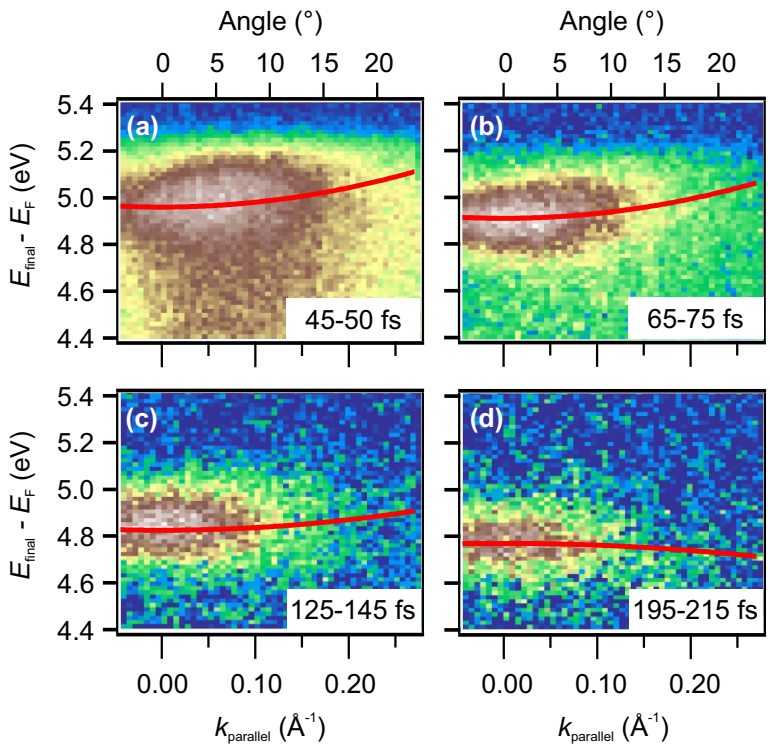

FIG. S5. Angle-resolved data after negative-time background subtraction for four different pump-probe delay time regions.

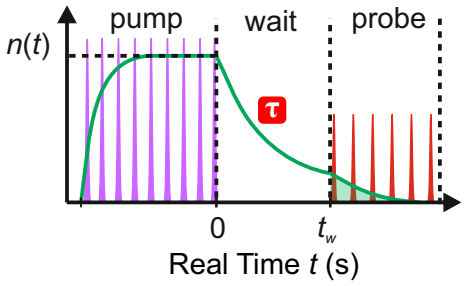

FIG. S6. A schematic of pump-wait-probe spectroscopy with 3.1 eV "pump" time which produces the steady state population n of P_2, a dark "wait" time during which the population decays with decay time τ, and the 1.55 eV "probe" time. .

using a train of 1.55 eV laser pulses, insufficient photon energy for population of P_2 but sufficient for photoemission from P_2. The 1.55 eV photoemission signal as a function of wait time provides a measure of the decay time, τ, of the long-lived electronic state. A pump time of 30 seconds was used to insure that a steady-state of P_2 was reached.

A probe time of 15 seconds was used to probe the population of P_2 after the wait time. The mathematics of the probe intensity as a function of wait-time is described in the following paragraphs. After the pump time, the population of P_2 has reached a steady-state, P_0. This then decays with a rate $k = 1/\tau$ and $dP_2/dt = -kP_2$. Therefore equation S7 describes the population of P_2 as a function of time.

$$P_2(t) = P_0 e^{-kt} \tag{S7}$$

After an arbitrary "wait" time, t_w, the population of P_2 that remains is,

$$P_2(t_w) = P_0 e^{-kt_w}. \tag{S8}$$

Now if during the probing time this was all photoemitted with the first laser pulse this would be the intensity of the probed signal. However, in the first laser pulse only a percentage of P_2 is photoemitted, which we will define as x. Therefore the measured photoemitted intensity from the first laser pulse is

$$P_2^1(t_w) = xP_0 e^{-kt_w} \tag{S9}$$

and the remaining population, under the assumption that the laser pulse does nothing to the population that is not photoemitted, is

$$P_2^{1r}(t_w) = (1-x)P_0 e^{-kt_w}. \tag{S10}$$

When the second laser pulse comes a time Δ later this remaining population has decayed by $e^{-k\Delta}$. Assuming that the percentage of P_2 that is photoemitted remains constant, the measured photoemission intensity from the second laser pulse is

$$P_2^2(t_w + \Delta) = x(1-x)P_0 e^{-k(t_w+\Delta)} \tag{S11}$$

and the remaining population is

$$P_2^{2r}(t_w + \Delta) = (1-x)(1-x)P_0 e^{-k(t_w+\Delta)}. \tag{S12}$$

Continuing with the same logic for the third and fourth laser pulses, the photoemission intensity with each subsequent laser pulse will be as follows:

$$P_2^3(t_w + \Delta) = x(1-x)^2 P_0 e^{-k(t_w+2\Delta)} \tag{S13}$$

$$P_2^4(t_w + \Delta) = x(1-x)^3 P_0 e^{-k(t_w+3\Delta)} \tag{S14}$$

The probing time is 15 seconds and continues well past the point where there is no detectable photoemission signal of P_2. The total probed signal from all of the laser pulses is summed together and defines the "probed" signal at a given wait time. This total probed signal (TPS(t_w)) is given by

$$\mathrm{TPS}(t_w) = P_2^1(t_w) + P_2^2(t_w + \Delta) + P_2^3(t_w + 2\Delta) + P_2^4(t_w + 3\Delta) + ... \tag{S15}$$

Plugging in the expressions above for $P_2^n(t_w + (n-1)\Delta)$ and simplifying,

$$\begin{aligned}\mathrm{TPS}(t_w) =& xP_0e^{-kt_w}\left[1 + (1-x)e^{-k\Delta} + (1-x)^2e^{-k2\Delta} + (1-x)^3e^{-k3\Delta}...\right] &\text{(S16)}\\ =& xP_0e^{-kt_w}\left[\lim_{n\to\infty}\left\{(1-x)e^{-k\Delta}\right\}^n\right] &\text{(S17)}\end{aligned}$$

The last term is a converging geometric series because $(1-x)e^{-k\Delta}$ must be less than 1 as $0 \leq x \leq 1$. This converges to

$$\lim_{n\to\infty}\left\{(1-x)e^{-k\Delta}\right\}^n = \frac{1}{1-(1-x)e^{-k\Delta}} = \frac{e^{k\Delta}}{x}. \tag{S18}$$

Therefore the expression for TPS(t_w) becomes

$$\mathrm{TPS}(t_w) = xP_0e^{-kt_w} \cdot \frac{e^{k\Delta}}{x} = P_0e^{-k(t_w-\Delta)} \tag{S19}$$

Measuring the population of the long-lived state as a function of waiting time with $\Delta = 5$ μs (laser repetition rate of 200 kHz) directly determines k and thus τ, the lifetime of the long-lived electronic state.

VII. MODEL FOR P_2 LIFETIME AS A FUNCTION OF DMSO COVERAGE

As discussed in the main paper, a model which takes into account both the wavefunction overlap-dependent probability of formation of P_2 as well as the distance-dependent tunneling back to the Cu substrate captures the overall trend in the P_2 lifetime with DMSO coverage. Due to the lifetime of P_2 that exceeds the inverse repetition rate, a steady-state population of P_2 will build up during the "pump" time. P_2 binding sites could be anywhere on the multilayer surface, however the steady-state population of P_2 will not be the same as a function of the distance from the 2nd monolayer if P_1 acts as a precursor state. The differential

equation that describes the population of P_2 as a function of time and distance z from the second monolayer is:

$$\frac{dP_2(z)}{dt} = S_{P_1P_2}(z)F_{pump}[N_z - P_2(z)] - \sigma_z F_{probe}P_2(z) - \frac{P_2(z)}{\tau(z)} \tag{S20}$$

where $S_{P_1P_2}(z)$ is the probability of electron transfer from P_1 to P_2, F_{pump} and F_{probe} are the pump and probe pulse fluences, N_z is the number of P_2 binding sites at distance z, σ_z is the photoemission probability from P_2, and $\tau(z)$ is the lifetime of P_2 at z. As discussed in detail in reference S7, a steady-state approximation can be used to find the steady-state population of P_2 as a function of z. The expression for this steady-state population $P_2^{SS}(z)$ is,

$$P_2^{SS}(z) = \frac{S_{P_1P_2}(z) \cdot N_z}{\sigma_z + S_{P_1P_2}(z)} \tag{S21}$$

where $F_{pump} = F_{probe}$ because 3.1 eV acts as both and $\tau(z)^{-1}$ has been neglected in comparison to the much higher probabilities of electron transfer and photoemission. For simplicity $S_{P_1P_2}(z)$ is modeled as an exponential $S_{P_1P_2}(z) = ce^{-z\zeta}$, where c is the probability of electron transfer at 2 monolayers and ζ is a measure of the decrease in the probability of electron transfer as a function of distance. Therefore $P_2^{SS}(z)$ has three independent variables, ζ, N_z, and σ_z/c.

$$P_2^{SS}(z) = \frac{e^{-z\zeta} \cdot N_z}{\sigma_z/c + e^{-z\zeta}} \tag{S22}$$

We assume that the number of trapping sites N_z and the photoemission probability σ_z do not change as a function of distance z and therefore that the main contribution to the distance-dependent steady-state population $P_2^{SS}(z)$ is the probability of electron transfer to P_2 governed by the wavefunction overlap with P_1.

As discussed in the main paper, the lifetime of P_2, $\tau(z)$, is most likely dependent upon the distance of P_2 from the Cu surface.[S7] In our simple model, we use an exponential dependence for $\tau(z)$,

$$\tau(z) = \tau_0 \exp(z\gamma), \tag{S23}$$

the most extreme case for lifetime enhancement as a function of distance, in order to ensure that even weakest distance dependences of $\tau(z)$ can result in the observation of a saturating average lifetime in the experiment. In equation S23, τ_0 is the lifetime for P_2 at 2 monolayers from the Cu surface and γ is a measure of the increase in lifetime as a function of distance. We can approximate the lifetime that we measure in the pump-wait-probe measurements at a

given average coverage i as a weighted average lifetime, $\langle\tau(i)\rangle$, of surface-bound electrons P_2. The weighting is due to the difference in the steady-state population $P_2^{SS}(z)$ as a function of distance. For higher average coverages, i, the weighted average is applied over larger available distances z as the average thickness is higher, shown in Equation S24.

$$\langle\tau(i)\rangle = \frac{\sum_{z=0}^{i-2} P_2^{SS}(z)\cdot\tau(z)}{\sum_{z=0}^{i-2} P_2^{SS}(z)} \approx \frac{\int_0^{i-2} P_2^{SS}(z)\cdot\tau(z)dz}{\int_0^{i-2} P_2^{SS}(z)dz} \tag{S24}$$

This expression for $\langle\tau(i)\rangle$ gives the curve shown in Figure 5(b) in the main paper where due to the drop-off in coupling between P_1 and P_2 with increasing distance we observe a saturation in the coverage dependent lifetime of P_2. The least squares fit of the model to the experimental points results in $\zeta = 0.46$ Å^{-1}, $\sigma/c = 0.06$, $\gamma = 0.38$ Å^{-1}, and $\tau_0 = 0.2$ s, where N_z drops out of equation S24.

REFERENCES

[S1]D. P. Woodruff and T. A. Delchar, *Modern Techniques of Surface Science*, 2nd ed. (Cambridge University Press, Cambridge, United Kingdom, 1994).

[S2]J.-C. Deinert, *Zeit- und Winkelaufgelöste Zweiphotonen-Photoemissionsspektroskopie: Aufbau und Charakterisierung des Experiments Anhand der Cu(111)- und der D_2O/Cu(111)-Oberfläche*, Diploma, Freie Universität Berlin (2011).

[S3]We observe a linear real-time decrease in the intensity of peak P_2 with photo-illumination. Neither the ultrafast dynamics nor the pump-wait-probe measurements of P_2 are effected by the intensity changes. Any real-time effects to the intensity of peak P_2 were mitigated in data collection by looping through pump-probe time delays in both the forward and reverse directions followed by summing both delay directions.

[S4]M. L. Strader, S. Garrett-Roe, P. Szymanski, S. T. Shipman, J. E. Johns, A. Yang, E. Muller, and C. B. Harris, J. Phys. Chem. C **112**, 6880 (2008).

[S5]D. Wegkamp, *Ultrafast Electron Dynamics and the Role of Screening*, Ph.D. thesis, Freie Universität Berlin (2014).

[S6]S. B. King, D. Wegkamp, C. Richter, M. Wolf, and J. Stähler, J. Phys. Chem. C **121**, 7379 (2017).

[S7]J. Stähler, M. Meyer, D. O. Kusmierek, U. Bovensiepen, and M. Wolf, J. Am. Chem. Soc. **130**, 8797 (2008).